Sustainable Chemistry for the Environment 3 (2023) 100026

Contents lists available at ScienceDirect

Sustainable Chemistry for the Environment

journal homepage: www.editorialmanager.com/scenv

Valorization of solid waste incinerator fly ash by geopolymer production for removal of anionic bromocresol green dye from water: Kinetics, isotherms and thermodynamics studies

Eugene K. Owino [a], Victor O. Shikuku [b,*], Wilfrida N. Nyairo [a], Chrispin O. Kowenje [a], Benton Otieno [c]

[a] Department of Chemistry, Maseno University, P.O. Box 333, Maseno 40105, Kenya
[b] Department of Physical Sciences, Kaimosi Friends University, P.O. Box 385-50309, Kaimosi, Kenya
[c] Centre of Renewable Energy and Water, Vaal University of Technology, Private Bag X021, Vanderbijlpark 1900, South Africa

ARTICLE INFO

Keywords:
Geopolymers
Solid waste incinerator fly ash
Valorization
Adsorption
Dyes

ABSTRACT

In this study, solid waste incinerator fly ash (SWI-FA) based geopolymer adsorbents were prepared by alkalination of hazardous SWI-FA and cured at different temperatures of 30 ^{0}C (GP30), 50 ^{0}C (GP50), 70 ^{0}C (GP70), and 90 ^{0}C (GP90). The geopolymers were applied as low-cost adsorbents for the removal of anionic bromocresol green (BCG) dye from water under varying conditions. The precursor and geopolymers were characterized by XRD, SEM-EDS, FT-IR, and point of zero charge (PZC). The geopolymers were morphologically different with varying chemical compositions. The kinetic data were best described by the pseudo second order model. The experimental equilibrium adsorption data were fitted to Langmuir, Freundlich, Temkin and Dubinin-Radushkevich-Kaganer adsorption isotherm models. The Langmuir monolayer maximum adsorption capacities increased consistently with curing temperature, from 41.70 mg/g to 515.5 mg/g for GP30 and GP90, respectively, a new benchmark for these materials for anionic dyes. The thermodynamic parameters, namely enthalpy ($\Delta H < 0$), Gibbs free energy ($\Delta G < 0$), entropy ($\Delta S > 0$) and activation energy (E_a) indicated that the processes are spontaneous, exothermic, physical ($E_a < 5$kJ/mol and $\Delta H < 40$kJ/mol) and enthalpy-driven. The adsorption mechanisms included strong electrostatic interactions and hydrogen bonding. The production of these geopolymers provides dual advantage of waste valorization with applications in depollution of water.

1. Introduction

Geopolymers are inorganic polymeric materials with amorphous or semi-crystalline structure synthesized by alkali or acid activation of aluminosilicate materials at temperatures below 100 ^{0}C [1]. A great variety of materials with silica and alumina content such as calcined kaolinite, feldspar, albite, clays, red mud, metakaolin, fly ash (FA), granulated blast furnace slag (GBFS), rice husk ash (RHA), volcanic ash, palm oil fuel ash (POFA) have been found suitable for geopolymer production [2,3]. Geopolymers have wide range of applications such as heavy metal and dye adsorption from wastewater, production of ceramics, in green construction and as adhesives among many others uses [4] Of particular interest is application of solid waste incinerator fly ash (SWI-FA) geopolymer in water treatment as a way of valorization of SWI-FA so as to fulfill the goal of zero waste and immobilization of its toxic constituents [5].

The frequent use of dyes by many industries to apply color to the substrate has led to water pollution. The presence of dyes in water raises serious environmental concerns since dyes are chemicals that are highly toxic and potentially carcinogenic to human beings [6]. A number of conventional water treatment approaches used to process polluted water into safe drinking water such as coagulation; flocculation, clarification and filtration that have been found to be insufficient in removing dyes from water at molecular levels. Alternative techniques such as advanced oxidation processes are very expensive and are known to form toxic by-products in the process of dye removal [7]. Adsorption is currently the most widely utilized technique in water treatment process since it can be used for removal of very low concentrations of water pollutants and also because of the ease of manipulation adsorption process. The most commonly used adsorbent for the removal of water pollutants is activated carbon since it is stable and possesses a higher surface area [8]. However, activated carbon is very expensive and the cost of

* Corresponding author.
E-mail address: vshikuku@kafu.ac.ke (V.O. Shikuku).

https://doi.org/10.1016/j.scenv.2023.100026
Received 4 April 2023; Received in revised form 21 July 2023; Accepted 23 July 2023
Available online 25 July 2023

regeneration is also very high [9]and this necessitates the search for new, efficient, eco-friendly and sustainable adsorbents from locally available materials, especially in the emerging economies [10]. Owing its porous structure, tunable nature and negative surface charge, geopolymers have shown very good performance in the removal of dyes from aqueous solution [4,11]. Due to the presence of SiO_2 and Al_2O_3, SWI-FA has been used as a raw material for the synthesis of a geopolymer adsorbent for removal of methylene blue (MB), a cationic dye from aqueous solution [12] and zeolites for the removal of heavy metals from aqueous solution [5]. Margallo et al. [13]. suggests that several treatments such as water washing and stabilization/solidification can be adapted to SWI-FA to help reduce the negative environmental effect of SWI-FA and obtain a new product, with a wide range of applications.

One of the main advantage of geopolymers is the ability to tune their textural, structural, morphological and compositional characteristics [14,15]. Structural and textural characteristics of geopolymers can be controlled by the precursor materials and preparation conditions (curing temperature, time etc.) [3]. For example, Li et al. [15] studied the effect of curing temperature on high-strength metakaolin-based geopolymer composite (HMGC) prepared by mixing different proportions of quartz powder and steel fiber. The study revealed that increase in curing temperature had a significant effect on structural, morphological and textural characteristics of the HMGC. Sajan et al. [16] also reported the effect of curing temperature on the morphological characteristics of fly ash based geopolymer. The study revealed that increase in curing temperature from 20 ^{0}C to 80 ^{0}C, results to change in the geopolymer morphology from a less dense to highly dense solid matrix and also a reduction in the pore size.

Structural, textural and compositional characteristics are important in determining adsorption rate and capacities of geopolymer adsorbents for specific pollutants [3]. These findings are crucial as they provide a clear guideline in establishing adsorption performance today. An understanding of the correlation between characteristics of geopolymer and their adsorption performance is key in setting up a practical water purification process [3]. Al Ghouti et al. [12] noted that the MSW-FA geopolymer adsorbent with a lower surface area of 4.5 m^2/g had a relatively lower adsorption capacity of 434.7 mg/g for methylene blue (MB) at 25 ^{0}C as compared to MSW-BA geopolymer adsorbent with a surface area of 32.78 m^2/g that had an adsorption capacity of 666.7 mg/g at 25 ^{0}C. Textural characteristics is an important criterion when selecting suitable adsorbents. Several approaches have been proposed for enhancing textural characteristics and adsorption density of geopolymers including the use of additives such as hydrogen peroxide, use of different activator solutions and variation of the composition of the aluminosilicate source [1,3,11]. Textural characteristics, however, is not the sole criterion for selecting suitable adsorbents since geopolymers with varying textural properties can have indistinguishable adsorption capacities [3]. Several works have also reported the influence of geopolymer composition on adsorption rate and capacity [2,3]. For instance, by partially replacing 0 %, 5 %, 10 % and 20 % pozzolan with sugarcane bagasse-derived biochar for production of geopolymer adsorbent, the uptake of methylene blue from aqueous solution decreased beyond 10 % inclusion of sugarcane bagasse [2]. The textural properties and composition of SWI-FA geopolymers are required for maximization of their adsorbing properties.

Previous research on the interaction of SWI-FA based geopolymer with water pollutant was reported only for cationic dye, MB [12] despite the widespread use of anionic dyes and their occurrence in wastewater. The suitability for SWI-FA based geopolymers for anionic dyes has not been documented. Since geopolymers bear a negative surface charge, there is need to optimize both their textural properties and composition to maximize the uptake of anionic dyes [1]. Thus, the objective of this work was to study the effect of curing temperature on textural, structural, morphological, composition and adsorption characteristics of SWI-FA based geopolymers for the removal of bromocresol green, a model anionic dye, from aqueous solution.

2. Materials and methods

2.1. Preparation of adsorbent

The aluminosilicate source, the solid waste incinerator fly ash (SWI-FA), obtained from the Environmental Combustion Ltd (Migori, Kenya) was sieved through 100-μm sieve to obtain uniform particle size. To prepare activator solution, 12 g of sodium silicate powder (18 wt% Na_2O, 63 wt% SiO_2, 19 wt% H_2O; SiO_2/Na_2O weight ratio of 3.5) was added to 15 mL of 8 M NaOH solution in polypropylene beaker, stirred for 30 min at 800 rpm to obtain a uniform mixture and stored for a 24hrs at room temperature. A mass of 30 g of SWI-FA was added to the 15 mL alkali activator solution and the mixture homogenized for 5 min using a mixer to produce a geopolymer paste. The produced geopolymer pastes were placed in closed containers and each cured for 24 h at different temperatures of 30 ^{0}C (GP30), 50 ^{0}C (GP50), 70 ^{0}C (GP70) and 90 ^{0}C (GP90). Excess NaOH was removed from the geopolymer samples by continuous washing with deionized water. The geopolymer samples were dried in an oven at 60 ^{0}C for 2 h, crushed, sieved through 100-μm sieve and stored in a desiccator.

2.2. Characterization of adsorbent

The crystalline phase of SWI-FA and SWI-FA based geopolymer samples was determined using X-ray Brucker diffractometer (D8 Advance) with copper radiation (K_α =1.5406). The morphology and microstructure of SWI-FA and the prepared SWI-FA based geopolymer samples was examined by Scanning Electron Microscope (JSM-IT500 InTouchScope™). The functional groups on the surface of geopolymer samples were determined by Fourier transform infrared spectrometry analysis using FT-IR spectrophotometer (Thermo Scientific™ Nicolet™ iS50) over the wavenumber range 4000 – 400 cm^{-1}. The pH of point zero charge was determined using the pH drift method.

2.3. Adsorption Experiments

2.3.1. Effect of initial concentration

The batch adsorption experiments were carried out in 250 mL Erlenmeyer flasks, each containing 50 mL of diluted bromocresol green dye (BCG) solutions at different concentrations (10, 20, 30, 40, 50 mg/L). A mass of 0.1 g of each SWI-FA geopolymer adsorbent was added to each reactor flask and the mixture stirred until equilibrium at pH 4, filtered and residual BCG in solution determined spectrophotometrically at 444 nm [31]. The equilibrium sorption capacity, q_e at different initial adsorbate concentration and percentage removal (%R) of BCG were obtained by the Eqs. (1) and (2) respectively.

$$q_e = \frac{(C_0 - C_e)V}{m} \quad (1)$$

$$(\%R) = \frac{C_0 - C_e}{C_0} \times 100 \quad (2)$$

Where:

C_0 The initial concentration BCG solution in mg/L
C_e The concentration of the residual BCG solution at equilibrium in mg/L
q_e The amount BCG solution in solid phase at equilibrium in mg/g,
$_m$ The mass of SWI-FAG adsorbent in g
V The volume of the liquid in litres

The treated effluent was analyzed for heavy metals (Pb, Cu, Cd, Mn, Cr, Fe and Zn) leaching from the geopolymer matrix using ICP-OES (Perkin Elmer Optima 3000 XL).

2.3.2. Effect of contact time

A mass of 0.1 g of each SWI-FA geopolymer adsorbent was added, in turn, to 50 mL of 50 mg/L BCG solution. The mixture in the sealed flasks were agitated at 200 rpm at pH 4 for 120 min using an overhead temperature-controlled shaker at 298 K. At time interval of 15, 30, 45, 60, 75, 90, 105 and 120 min, the mixtures in the sealed flasks were filtered and residual BCG in solution determined. The amount of bromocresol green dye (BCG) adsorbed onto SWI-FAG, q_t, at any given time (t), was calculated using Eq. (3):

$$q_t = \frac{(C_0 - C_e)V}{m} \quad (3)$$

2.3.3. Effect of pH

The effect of pH was evaluated by varying the pH of 50 mL of 50 mg/L BCG solutions from 2 to 10 using aqueous 0.1 M NaOH and 0.1 M HCl depending on the desired pH. A fixed mass of 0.1 g of each of each SWI-FA geopolymer adsorbent was added, in the solutions with adjusted pH. The mixture in the flasks were agitated at 200 rpm for 60 min using an overhead temperature-controlled shaker at 298 K and the residual dye concentration determined.

2.3.4. Effect of temperature

A fixed mass of 0.1 g of each SWI-FA geopolymer adsorbent was added, in turn, to 50 mL of 50 mg/L BCG solutions in sealed 250 mL Erlenmeyer flasks at pH 4. The temperature of the contents of the sealed flasks were adjusted to 298, 323, 343, 353, 363 K, agitated until equilibrium and the residual dye concentration determined.

3. Results and discussion

3.1. Point of zero charge

The pH of point of zero charge is an index of the surface charge of the adsorbent at different solution pH. Fig. 1 shows the plot for the point of zero charge of SWI-FA based geopolymers (GP30, GP50, GP70 and GP90. The point of zero charge (pH_{PZC}) of the SWI-FA geopolymer adsorbents was found to be 6.8. This suggests that the SWI-FA geopolymer adsorbents surface charges were indistinguishable and become positively charged at solution pH below pH 6.8, neutral at solution pH of 6.8 and negatively charged at solution pH above 6.8. The pHpzc was unaffected by curing temperature.

3.2. Functional group analysis

Fig. 2 shows FTIR spectra for SWI-FA and SWI-FA based geopolymers (GP30, GP50, GP70 and GP90) before adsorption of BCG. A comparison of the spectra of the geopolymers with that of SWI-FA revealed some changes in the bands. The band at 991 cm^{-1} assigned to the asymmetric stretching vibrations of Si-O-T (T-tetrahedral Al or Si) in SWI-FA [17] shifted to lower wavenumber of 971 cm^{-1} (GP30), 975 cm^{-1} (GP50), 971 cm^{-1} (GP70), 988 cm^{-1} (GP90) in the geopolymers. The shift and

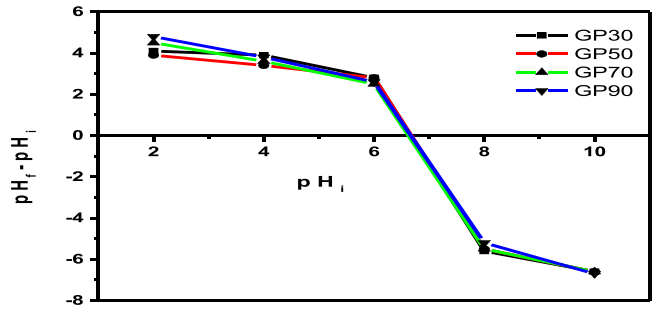

Fig. 1. Point of zero charge of SWI-FA geopolymer.

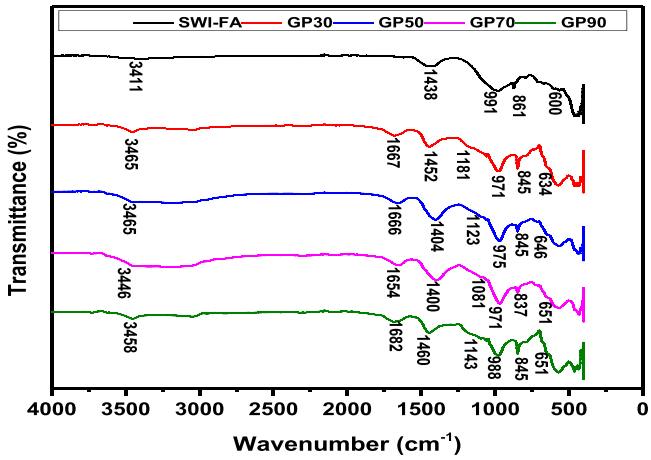

Fig. 2. FT-IR spectrum for SWI-FA and SWI-FA based geopolymers (GP30, GP50, GP70 and GP90).

narrowing of band at 991 cm^{-1} suggests rearrangement of Si-O-Si, Si-O-Al and Al-O-Si bonds present in aluminosilicate raw source and their involvement in geopolymerization would result in formation of new polymeric bonds [18]. Conversely, these changes were also as a result of increase in the Si-O-T bond length and reduction of bond angle causing a decrease in molecular vibrational force constant in the geopolymer gel [14,19]. A similar trend in FT-IR analysis have been reported in geopolymer production studies by Sivasakthi et al. [19] as confirmation of the successfully synthesis of a geopolymer [14]. Comparing the shift of the band at 991 cm^{-1} and the geopolymer cured at 90^0 C (GP90), the absorption band shifted to 988 cm^{-1}, an indication that elevating curing temperature influences the SWI-FA dissolution in the alkaline activator solution favoring geopolymerization [20–22]. The bands between 1682 and 1654 cm^{-1} and 3465 – 3411 cm^{-1} represent the stretching and deformation vibrations of H-O-H and -OH bonds in GP30, GP50, GP70 and GP90 a characteristic of bonds in water molecule and silanol group [17]. The band centered between 600 and 861 cm^{-1} indicated the presence of deformation vibration of Si-O-T in SWI-FA, GP30, GP50, GP70 and GP90 [17]. The band at 1387 cm^{-1} in the spectrum of the BCG-laden geopolymer (Fig. 3) attributed to the symmetric bending vibration of $-CH_3$ group [2], evidence of BCG adsorption on the surface of geopolymer adsorbent. In addition, the narrowing of band due to -OH bond (3280 cm^{-1}) and elongation of band at 965 cm^{-1} (Fig. 3) associated with the asymmetric stretching vibrations of Si-O-T (T-tetrahedral Al or Si) is possibly due to modifications associated with conjugation of BCG on the surface of the GP70 geopolymer adsorbent.

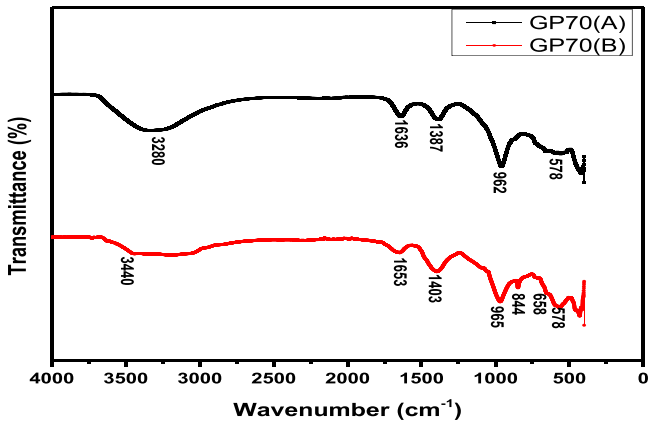

Fig. 3. FT-IR spectrum for GP70 before and after adsorption.

3.3. Mineralogical (XRD) analysis

Fig. 4 and Fig. 5 shows XRD patterns of SWI-FA (aluminosilicate source) and the SWI-FA based geopolymers GP50, GP70 and GP90, respectively. The SWI-FA is made up in quartz, syn, SiO_2 (ICSD 01–083–2433), calcite, $CaCO_3$ (ICSD 01–086–2342), kyanite, Al_2SiO_5 (ICSD 01–072–1441) and gehlenite, syn, $Ca_2Al(AlSiO_7)$ (ICSD 01–087–1275) as crystalline phases. These crystalline phases of SWI-FA were not observed in the SWI-FA based geopolymers, an indication that these phases completely dissolved and reacted in the alkaline activator solution. The XRD patterns shows that the main crystalline phases of the SWI-FA based geopolymers under different curing temperatures are basically the same. This is an indication that increasing curing temperature had no significant effect on the chemical composition or phase evolution of SWI-FA based geopolymer [15]. The XRD patterns of the SWI-FA based geopolymers shows the appearance of grossular, $Al_2Ca_3(SiO_4)_3$(ICSD 01–074–1088) and albite, $Na(AlSi_3O_8)$ (ICSD 01–084–0752) in GP30, GP50, GP70 and GP90; anorthite, $CaAl_2Si_2O_8$ (PDF 00–041–1486) in GP70 and GP90 and tilleyite, $Ca_5Si_2O_7(CO_3)_2$ in GP30 and GP50 which were not present in SWI-FA. The amorphous phase shown by a hump is observed in the SWI-FA and SWI-FA based geopolymer samples around $2\theta = 20^0 - 40^0$region. However, GP30 has a lower crystallinity index of 68.73 % as compared to that of SWI-FA at 86.97 %, an indication that the amorphous gel formation occurred during geopolymerization [2]. The XRD analysis reported in this work agrees with the outcomes reported in other research [15].

3.4. Morphological and elemental analysis

Fig. 6. shows the SEM micrographs depicting the microstructural analysis results for SWI-FA, GP30, GP50, GP70 and GP90 at different magnifications using scanning electron microscopy (SEM). Fig. 6A shows SWI-FA morphological structure consisting of tiny spherical particles which are packed together and appears to be highly porous. Figs. 6B to 6E shows that all the SWI-FA based geopolymer adsorbents (GP30, GP50, GP70 and GP90) consists of non-uniform surfaces with small spherical particles of unreacted SWI-FA fused together with a dense geopolymer gel-like matrix, an indication of a moderation reaction in the geopolymer system. However, Fig. 6C shows a geopolymer sample with a less dense matrix compared to other geopolymer sample. In addition, the SWI-FA based geopolymers possessed porous surfaces, which are vital in dye adsorption [4]. The SEM images of the geopolymers revealed morphologies different from that of SWI-FA, where the gaps between the SWI-FA particles are filled with a geopolymer gel. It was evident from Figs. 6B to 6E that GP30, GP50, GP70 and GP90

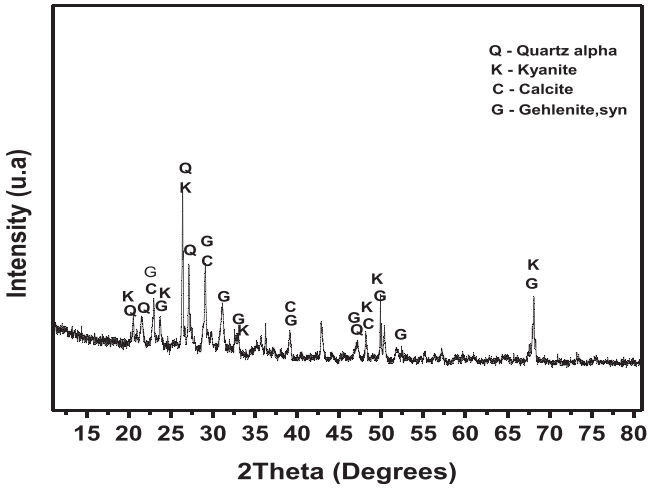

Fig. 4. X-ray diffraction (XRD) pattern of the SWI-FA.

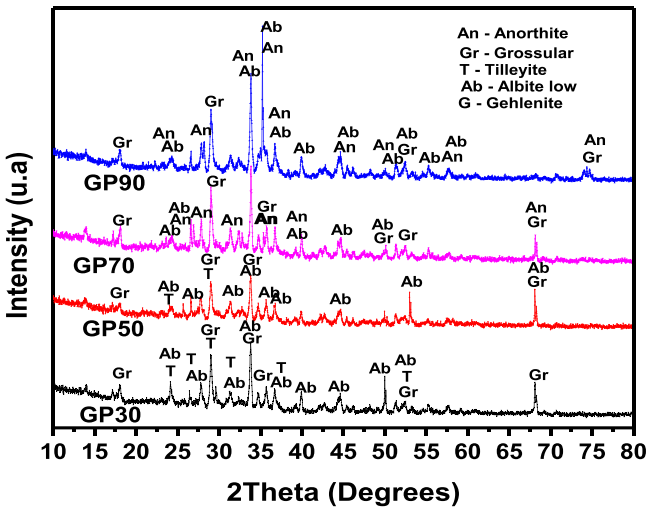

Fig. 5. X-ray diffraction (XRD) pattern of the SWI-FAG under different curing temperatures.

consisted of spongy and gel -like structure with uniform granules, a confirmation that geopolymerization of SWI-FA was successful [12]. This results confirms the FT-IR analysis findings which indicated the formation of a geopolymer. The results of microstructural analysis of the SWI-FA based geopolymer is similar to those of fly ash based geopolymers reported by Sajan et al. [16]. The elemental composition of SWI-FA, GP30, GP50, GP70 and GP90 were obtained by Energy-dispersive X-ray spectroscopy (EDS) analysis. In SWI-FA, elements C, O, Al, Si and Ca were detected. In-addition to C, O, Al, Si and Ca, the SWI-FA based geopolymers (GP30, GP50, GP70 and GP90) also had Na from the activator solution. From the EDX analysis (Table 1), the elemental composition of the SWI-FA based geopolymers (GP30, GP50, GP70 and GP90) reflects the suitability of SWI-FA as an aluminosilicate source. The SWI-FA based geopolymers cured at higher temperatures had a higher Si/Al ratio. During the curing process, increase in curing temperature caused increase in the rate of dissolution of aluminium and silicon from the SWI-FA resulting to a greater Si/Al ratio in geopolymer synthesized at 70 ^{0}C (GP70) then the rates are decreased when the geopolymer system reaches a supersaturated state [23].

3.5. Effect of pH

pH is one of the most important parameter in sorption process. Changes in pH impacts BCG removal efficiency and an adsorbent's adsorption capacity [9]. As shown in Fig. 7, increase in pH from 2 to 10 decreased the adsorption capacity of BCG onto the geopolymers. For instance, adsorption capacity of BCG onto GP90 decreased from 18.63 (75 % removal) to 4.70 mg/g (19 % removal) as the pH was increased from 2 to 10 and the highest adsorption capacity was obtained at pH 2. At pH below 6.8 (pH< pH_{PZC}) the surface of SWI-FA geopolymer becomes more positively charged because of protonation of aluminol and silanol species on the surface of SWI-FA geopolymer (i.e. $Al-OH + H^+ \rightleftharpoons Al-OH_2^+$). The adsorption of anionic BCG dye onto SWI-FA geopolymers is favored due to strong electrostatic attraction between the negatively charged anionic BCG and the positively charged aluminol and silanol sites on the geopolymer surface. This is consistent with the conjugation of BCG molecules on the surface of SWI-FA geopolymer as described by FT-IR results (Fig. 3.). The favorable adsorption of BCG at lower pH may also be due to hydrogen bonding. Under acidic conditions, the protonated aluminol and silanol species on the surface of SWI-FA geopolymer and the monoanionic form of BCG may act as hydrogen acceptor and donor respectively. Above pH 6.8 (pH>pH_{PZC}), the surface of the SWI-FA geopolymer has an overall negative charge which resulted in electrostatic repulsion between the BCG molecules and the negatively

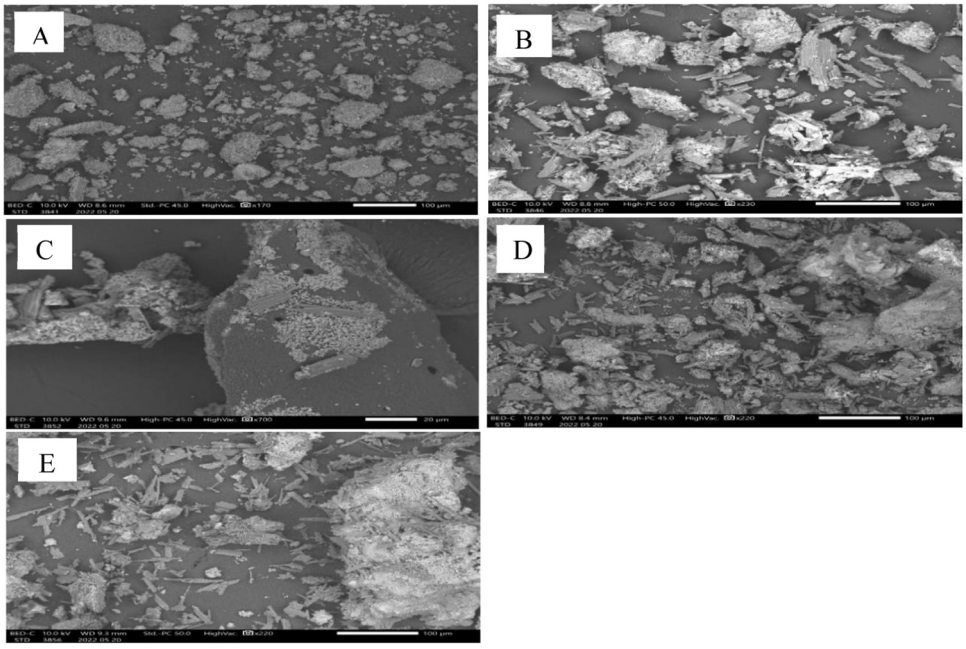

Fig. 6. SEM images of SWI-FA (A); GP30 (B); GP50 (C); GP70 (D); GP90 (E).

Table 1
EDS analysis of SWI-FA, GP30, GP50, GP70 and GP90.

	Elements	C	O	Na	Al	Si	Ca	Si/Al
SWI-FA	% Mass	48.55	34.90	-	2.99	5.51	8.04	1.84
GP30	% Mass	41.14	42.77	11.01	1.35	2.61	1.13	1.93
GP50	% Mass	64.31	24.89	4.87	1.73	3.13	0.70	1.81
GP70	% Mass	29.59	46.83	16.00	1.75	4.74	1.10	2.71
GP90	% Mass	9.09	55.82	23.30	2.47	5.40	3.93	2.19

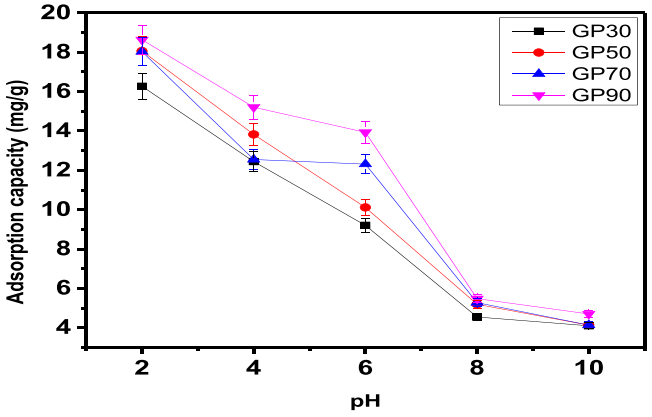

Fig. 7. Influence of pH on adsorption capacity of different SWI-FA geopolymers.

charged geopolymer resulting to a lower adsorption capacity. Additionally, an increase in pH above 6.8 resulted to increase in the concentration of hydroxide ions OH^-, which increased competition between BCG molecules and hydroxide ions (OH^-) for the active sites of the SWI-FA geopolymer. It is also notable that a considerable amount of BCG was still adsorbed onto SWI-FA geopolymer in the pH range from 8 to 10, an indication that other mechanisms, such as van der Waals interactions, besides electrostatic attraction are involved in the adsorption process. The sharp decrease in adsorption capacity with rise in pH shows that the electrostatic interactions are much stronger than the physical interactions. A similar result was observed by Liu et al. [24] during the uptake of BCG by chitosan poly(methacrylate) composites from aqueous solution.

3.6. Effect of contact time

The effect of contact time, between 0 and 120 min, on BCG adsorption onto GP90, GP70, GP50 and GP30 were studied at room temperature at pH 4 (Fig. 8). For all the sorbents, the adsorption capacity increased with increase in contact time. A comparison of the four geopolymers revealed that an equilibrium was reached within 60 min but they had different adsorption capacities. Beyond 60 min there was no appreciable change in the adsorption capacity.

3.7. Effect of initial concentration

The effect of initial BCG concentration on adsorption capacity was investigated and is presented in Fig. 9. The amount of BCG adsorbed on the SWI-FA geopolymer adsorbent increased with increase in initial BCG concentration depicting that mass transfer is the driving force for the migration of BCG from the bulk solution to the adsorbent surface [25]. The equilibrium adsorption capacity,q_e, increased from 3.019 mg/g to 15.21 mg/g (60.83 %), 2.464–12.4 mg/g (50.19 %), 2.905–13.82 mg/g (55.29 %) and 2.483–12.44 mg/g (49.77 %) for GP90, GP70, GP50 and GP30 when the initial concentration was increased from 10 to 50 mg/L, respectively. The increase in adsorption implies availability of more energetically favorable adsorption sites.

3.8. Kinetic study

The adsorption dynamics of BCG onto SWI-FA geopolymer adsorbents was analyzed using the pseudo-first order (PFO) kinetic model

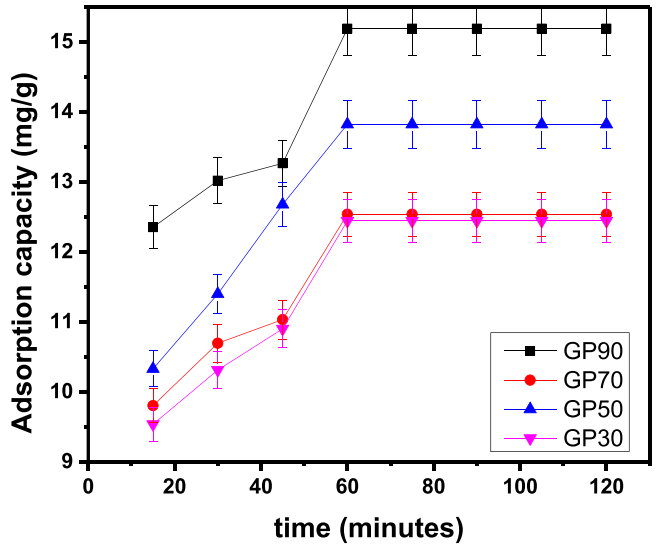

Fig. 8. Effect of contact time on adsorption capacities of different SWI-FA geopolymers.

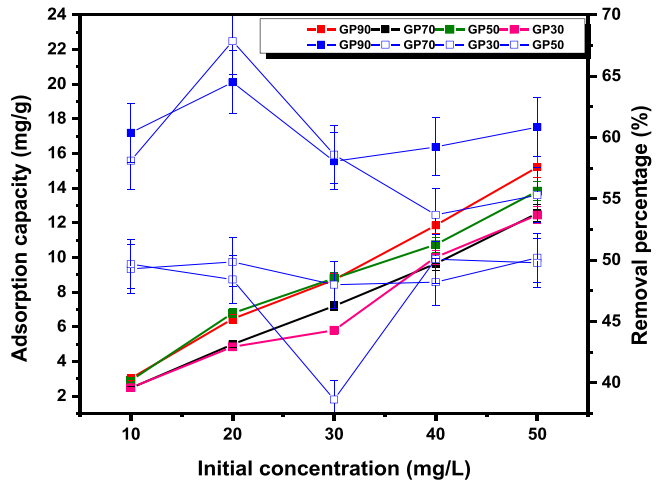

Fig. 9. Effect of initial BCG concentration on adsorption capacities of different SWI-FA.

[26] and pseudo-second order (PSO) kinetic model [27]shown in Eq. (4) and Eq. (5) respectively.

$$\text{Pseudo first order model}: \ln(q_e - q_t) = \ln q_e - k_1.t \quad (4)$$

$$\text{Pseudo second order model}: \frac{t}{q_t} = \frac{1}{k_2 q_e^2} + \frac{1}{q_e}.t \quad (5)$$

Where q_e is the amount of the adsorbate in mg.g^{-1} at equilibrium and q_t is the amount of the adsorbate in mg.g^{-1} at time t (min); $K_1$is the pseudo first order rate constant, min^{-1} and K_2 is the pseudo second order rate constant, mg.g^{-1}.min^{-1}.

The adsorption half-lives ($t_{\frac{1}{2}}$) were derived from the PFO and PSO regression plots (Fig. 10) using Eq. (6) and Eq. (7) respectively.

$$t_{\frac{1}{2}} = \frac{\ln 2}{K_1} \quad (6)$$

$$t_{\frac{1}{2}} = \frac{1}{K_2 q_e}. \quad (7)$$

The initial adsorption rate, S_{rate} (mg.g^{-1}.min^{-1}) were derived from the PFO and PSO regression plots using Eq. (8) and Eq. (9) respectively;

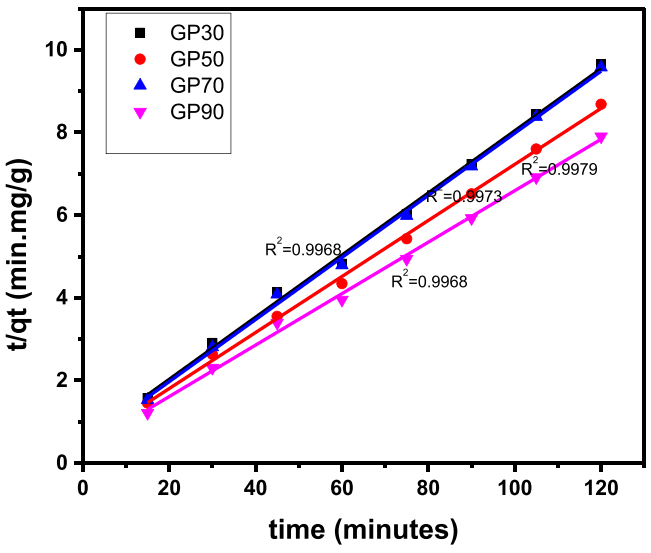

Fig. 10. Pseudo -second-order kinetic graph for adsorption of BCG onto SWI-FA geopolymers.

$$S_{rate} = k_1 q_e \quad (8)$$

$$S_{rate} = k_2 q_e^2 \quad (9)$$

To predict the rate-limiting steps, intra-particle diffusion model [28], Eq. (10) was fitted with the experimental data.

$$\text{Intra} - \text{particle diffusion model}: q_t = k_D t^{0.5} + C_B \quad (10)$$

Where, q_t is the amount dye adsorbed at time t (min), k_D (mg.g^{-1}.min$^{-1/2}$) is the intra-particle diffusion rate constant while C_B is a constant representative of the thickness of the boundary layer.

If the plot of the values of q_t against $t^{0.5}$is linear, then diffusion occurs through the pores of the adsorbent, and if the plot passes through the origin, then intra-particle diffusion is the only rate- limiting step. Positive C_B values illustrate a boundary layer effect, negative $C_B$values imply boundary layer has no effect on the rate of adsorption while larger values of C_B implies the external surface of the adsorbent has a greater contribution on adsorption [25,29]. Fig. 11 shows that the data of adsorption BCG onto SWI-FA geopolymer exhibited multi-linear plots could be divided into three linear regions to suggest that there are multiple stages to the adsorption process. In stage*I*, the adsorption capacity increased rapidly due to availability of more adsorption sites on the surface of the SWI-FA based geopolymer adsorbent. In stage*II*, the adsorption rate of BCG molecules was slower as compared to stage*I*. This is due to saturation of the available adsorption sites on the external surface of the adsorbent. In stage*III*, the adsorption equilibrium was reached [30]. The plots do not pass through the origin indicating that intra-particle diffusion is not the only rate-limiting step.

The best fitting kinetic model was determined by the coefficient of determination (R^2) values and comparing adsorption capacity predicted from the kinetic model and the experimentally determined values. The PFO had a lower R^2 values relative to the PSO model with R^2 values closest to 1. The predicted adsorption capacity values $q_{e(cal)}$ by PSO model (mg/g) were also very close to the experimentally adsorption capacity $q_{e(exp)}$ determined values as shown in Table 2. Therefore, the adsorption kinetics was best predicted by the pseudo-second order model (Fig. 10). The pseudo-second order model postulates that the adsorption rate of a solute onto an adsorbate depends on the adsorption capacity of the adsorbate and the rate-determining step is a chemisorption mechanism [31]. The half-life values indicate GP90 exhibited a relatively faster adsorption of BCG through a minimal variance. It appears that the adsorption rate, denoted by K_2 were practically

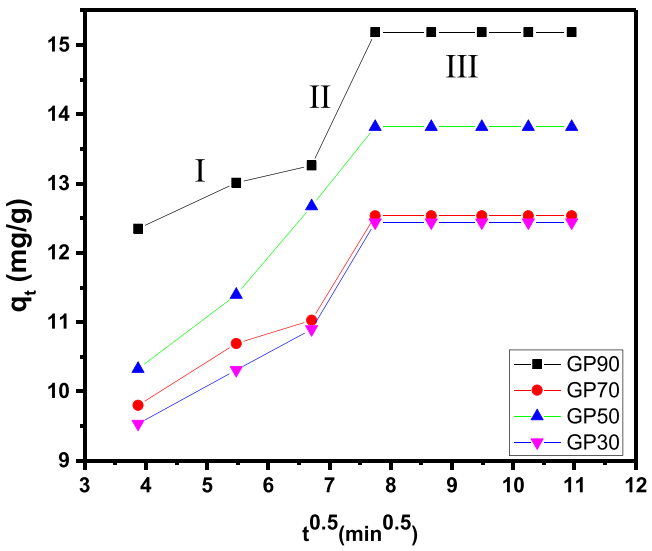

Fig. 11. Weber and Morris intra-particle diffusion plots.

Table 2
Kinetic parameters for removal of BCG onto SWI-FA geopolymer adsorbents.

Model	Parameter	GP30	GP50	GP70	GP90
PFO	K_1 (min^{-1})	0.0833	0.0842	0.0632	0.0564
	q_e (cal) (mg g^{-1})	7.8129	8.2763	5.3612	5.5448
	q_e (exp) (mg g^1)	12.439	13.819	12.534	15.186
	S rate (mg.g^1.min^{-1})	0.6510	0.6965	0.3390	0.3127
	$t_{\frac{1}{2}}$ (min)	8.319	8.237	10.961	12.290
	R^2	0.6852	0.6966	0.6890	0.6834
PSO	K_2 (g mg^1 min^1)	0.0107	0.0102	0.0112	0.0106
	q_e(cal) (mg g^{-1})	13.31	14.75	13.33	16.06
	q_e(exp) (mg g^1)	12.44	13.82	12.53	15.19
	S rate (mg.g^1.min^{-1})	1.9014	2.2266	2.1314	2.7331
	$t_{\frac{1}{2}}$ (min)	7.002	6.626	6.253	5.877
	R^2	0.9968	0.9979	0.9973	0.9968

indistinguishable and therefore unaffected by the morphological, textural or compositional differences between the geopolymers. However, adsorption kinetics is not the sole criterion for distinguishing between adsorbents. Shikuku et al. [3] demonstrated that geopolymers should have distinguishable and selected using both adsorption rates and adsorption capacities.

3.9. Adsorption isotherm

In this study, the experimental equilibrium adsorption data were fitted to Langmuir, Freundlich, Temkin, Dubinin-Radushkevich-Kaganer isotherm models (Fig. 12A-D) and their calculated constants and corresponding coefficients of determination (R^2) values are listed in Table 3. The dimensionless separation factor value, R_L, an index of the favorability of the adsorption process, was calculated by Eq. (11).

3.9.1. Langmuir isotherm

The Langmuir isotherm [32]assumes that a monolayer adsorption of adsorbate molecules can occur on a homogeneous adsorbate surface with identical sites and with minimal interaction between adsorbed molecules. The Langmuir isotherm is represented in the linear form by Eq. (11):

$$\frac{1}{q_e} = \frac{1}{K_L q_m}.\frac{1}{C_e} + \frac{1}{q_m} \tag{11}$$

Where, C_e is the concentration of dye at equilibrium in mg/L, q_e is the amount of adsorbed dye by SWI-FAG adsorbent at equilibrium in mg.g^{-1}, q_ms the single layer maximum adsorption capacity (mg.g^{-1}), and K_L (L/g) is the Langmuir constant connected to free energy of adsorption. The dimensionless separation factor was calculated by Eq. (12),

$$R_L = \frac{1}{1 + K_L C_o} \tag{12}$$

Where, K_L (L/mg) is the Langmuir constant connected to free energy of adsorption and C_0 is the initial BCG concentration (mg/L).

3.9.2. Freundlich isotherm

The Freundlich isotherm [33] is an empirical equation considered for multilayer adsorption, which occurs on a heterogeneous adsorbent surface and active sites with uniform energy. The Freundlich isotherm is represented in the linear form by Eq. (13):

$$\log q_e = \frac{1}{n} \log C_e + \log K_F \tag{13}$$

Where, K_F (L.g^{-1}) is the Freundlich constant of relative adsorption capacity of the SWI-FA based adsorbent in mg/g and $\frac{1}{n}$ is the constant of intensity of the adsorption.

3.9.3. Dubinin-Radushkevich-Kaganer (D-R-K) isotherm

The D-R-K model was applied to the adsorption process to estimates the porosity free energy of adsorption and distinguishes between physical or chemical nature of adsorption onto homogeneous and heterogeneous surfaces. The linear form of the D-R-K model is represented by Eq. (12):

$$\ln q_e = \ln q_m - k_D \xi^2 \tag{14}$$

Where, k_D is the Dubinin-Radushkevich-Kaganer isotherm constant in (mol^2/kJ^2), q_e is the amount of adsorbed dye by SWI-FAG adsorbent at equilibrium in mg.g^{-1} and q_m is theoretical monolayer saturation capacity (mg.g^{-1}) [34]. The Polanyi potential (ξ)is given by:

$$\xi = RT \ln\left(1 + \frac{1}{C_e}\right) \tag{15}$$

The mean adsorption energy E_a (kJ/mol) gives information on physical and chemical interactions between the adsorbate and adsorbent during the adsorption process.

$$E_a = \frac{1}{\sqrt{2k_D}} \tag{16}$$

3.9.4. Temkin isotherm

The Temkin isotherm equation presumes that the heat of adsorption of all the molecules in the layer would decrease linearly with coverage due to adsorbent/adsorbate interaction [35]. The adsorption is described by a uniform distribution of binding energies, up to some maximum binding energy. The Temkin isotherm model is given by equation

$$q_e = B_T \ln A_T + B_T \ln C_e \tag{17}$$

Where, $BT = \frac{RT}{bT}$, b (J/mol) is the Temkin constant related to the heat of adsorption; A (L/g) is the Temkin isotherm constant. R is the universal gas constant (8.314 J/mol/K), and T (K) the absolute temperature.

The isotherm plots are depicted in Fig. 12. Based on the coefficient of determination (R^2) values, the adsorption isotherms fitted the data in order Langmuir>Freundlich>Temkin>D-RK (Table 3). The separation factor R_L, were between $0 < R_L < 1$ for all geopolymers, indicating that the adsorption processes were favorable [2]. The magnitude of Freundlich constant *n* were above 1. The *n*values greater than 1 suggests the adsorption of BCG onto the geopolymers was a physical process [12] and whereas the values of $\frac{1}{n}$ in this study were below unity indicating a

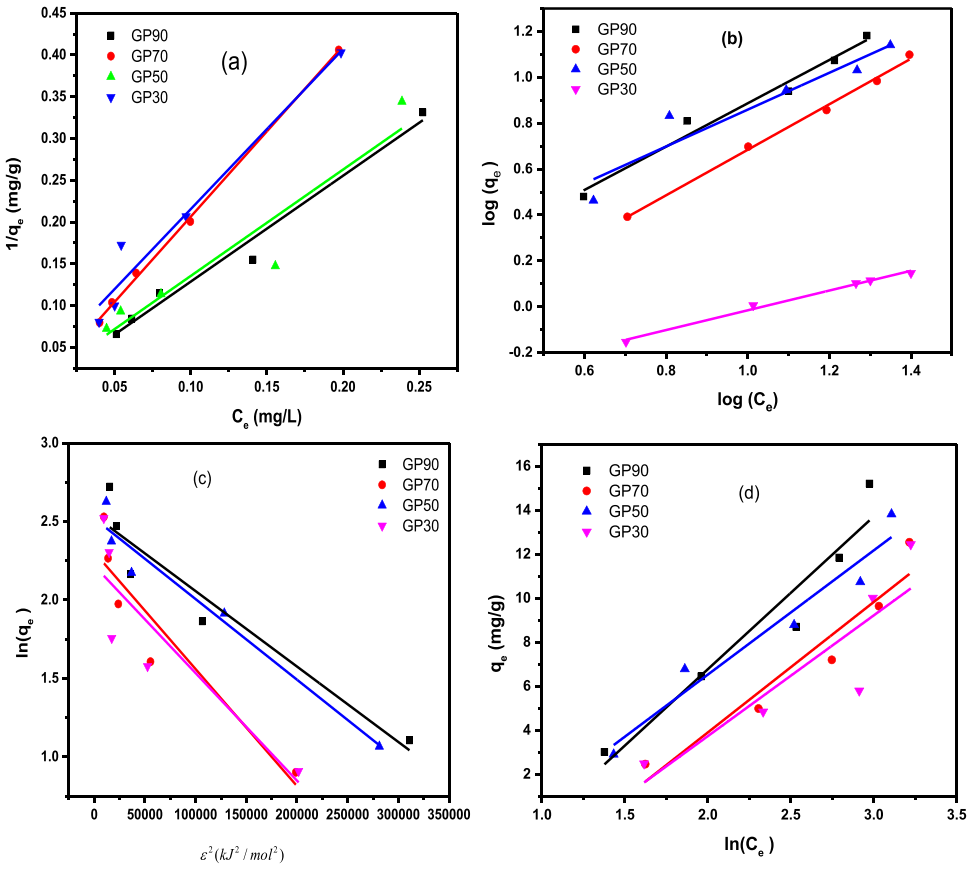

Fig. 12. (a) Langmuir (b) Freundlich (c) D-R-K (d) Temkin adsorption isotherm models.

Table 3
Parameters obtained from adsorption isotherm.

Isotherm	Parameter	GP30	GP50	GP70	GP90
Langmuir	q_{max} (mg/g)	41.70	121.8	452.5	515.5
	$K_{L\ (L/mg)}$	0.01252	0.00645	0.00108	0.00153
	R_L	0.6150	0.7561	0.9487	0.9289
	R^2	0.9435	0.8668	0.9982	0.9751
Freundlich	$K_{F\ (mg/g)(L/mg)^{-1}}$	0.3576	1.1359	0.4912	0.8746
	$\frac{1}{n}$	0.4308	0.8039	0.9929	0.9451
	n	2.3213	1.2440	1.007	1.0581
	R^2	0.9896	0.8695	0.9950	0.9685
Temkin	A_T (L/g)	0.2674	0.4307	0.2615	0.3594
	B_T (kJ/mol)	5.4885	5.6423	5.9253	6.9383
	R^2	0.7010	0.9257	0.8993	0.9041
D-R-K	q_{max} (mg/g)	9.1915	12.413	10.016	12.637
	E_a(kJ/mol)	0.2702	0.3120	0.2590	0.3226
	R^2	0.6937	0.9452	0.8321	0.8827

strong adsorbent-adsorbate interactions [36]. From Langmuir isotherm model the maximum adsorption capacity for BCG dye uptake increased with curing temperature in the order GP30 (41.70 mg/g) < GP50 (121.8 mg/g) <GP70 (452.5 mg/g) <GP90 (515.5 mg/g). The values of the activation energies E_a obtained from the D-R-K isotherm model were below 8 kJ/mol corresponding to a physisorption mechanism [2]. The Freundlich affinity constant (K_F) did not follow any logical sequence with increase in curing temperature. This implies that the increase in adsorption capacity with increase in curing temperature cannot solely be attributed to increased affinity between the adsorbent and the adsorbate. The interactions are therefore complex relating to both composition and textural characteristics of the geopolymers, both of which are influenced by curing temperature.

4. Adsorption thermodynamics

The effect of temperature on the adsorption of BCG onto GP90, GP70, GP50 and GP30 was evaluated in the temperature range from 298 to 363 K to determine the nature of adsorption. The thermodynamic parameters, namely, change in Gibbs free energy (ΔG), enthalpy (ΔH) and entropy (ΔS) were estimated using the following equations.

$$\Delta G^0 = -RT \ln K_C \tag{18}$$

$$K_d = \frac{C_{ad}}{C_e} \tag{19}$$

$$K_C = 1000 K_d \tag{20}$$

$$\ln K_C = \frac{\Delta S}{R} - \frac{\Delta H^0}{RT} \tag{21}$$

Where, K_C is the equilibrium constant (dimensionless), C_e is concentration of the residual BCG solution at equilibrium in mg/L and C_{ads} is the amount BCG solution in solid phase at equilibrium in mg/g, K_d is the distribution coefficient in L/g and the density of water is 1000 g/L.

The negative values of ΔG° and ΔH (Table 4) indicates that adsorption of BCG on SWI-FA geopolymers is a spontaneous and exothermic process, respectively. Generally, the computed ΔG° values could indicate whether an adsorption process is either physisorption for $-20 < \Delta G^\circ < 0$ kJ/mol or chemisorption for $-400 < \Delta G^\circ < -80$ kJ/mol [31,39]. The calculated ΔG° values (Table 4) for adsorption of BCG onto SWI-FA based geopolymer were in the range from −15.38 to −18.51 kJ/mol, indicating adsorption process entailed a physisorption mechanism. The positive values of entropy (ΔS) shows an increased disorderliness at the solid-liquid interface during BCG adsorption. Additionally, the ΔH values were below 40 kJ/mol, an index that the adsorption of BCG onto

Table 4
Thermodynamic parameters for BCG adsorption onto SWI-FA Geopolymer.

Geopolymer	Temp (K)	ΔG (kJ/mol)	ΔH (kJ/mol)	ΔS (kJ/mol/K)	E_a (kJ/mol)	S^*
GP30	298	-15.38	-5.915	32.02	3.262	0.1361
	323	-16.40				
	343	-16.95				
	353	-17.17				
	363	-17.47				
GP50	298	-15.92	-6.196	32.87	3.102	0.1607
	323	-16.90				
	343	-17.59				
	353	-17.78				
	363	-18.02				
GP70	298	-15.42	-6.044	31.47	3.348	0.1305
	323	-16.13				
	343	-17.05				
	353	-17.17				
	363	-17.33				
GP90	298	-16.49	-7.343	30.74	3.339	0.1591
	323	-17.31				
	343	-18.17				
	353	-18.51				
	363	-18.51				

the SWI-FA geopolymer adsorbent is a physical process [2]. This corresponds with the ΔG values and the deductions from the D-R-K model.

To further support the assertion that physisorption is the predominant mechanism, the value of activation energy (E_a) and sticking probability (S^*) were estimated from the experimental data. They were calculated using a modified Arrhenius type equation related to surface coverage as follows:

$$S^* = (1-\theta)e^{\frac{-E_a}{RT}} \tag{22}$$

$$\ln(1-\theta) = \ln S^* + \frac{E_a}{RT} \tag{23}$$

The value of θ was calculated from the following relation:

$$\theta = \left(1 - \frac{C_e}{C_0}\right) \tag{24}$$

The sticking probability (S^*)is a function of the adsorbent-adsorbate system whose value lies in the range $0 < S^* < 1$and is dependent on the temperature of the system. The parameter. indicates the measure of the potential of the adsorbate to remain on the adsorbate indefinitely [10]. In general, a physisorption mechanism has activation energies (E_a) in the range of 5–40 kJ/mol, whereas higher activation energies (40 −800 kJ/mol) denote a chemisorption process [24].

In this study, the values of $E_a$for adsorption of BCG onto SWI-FA geopolymer were in the range from 3.076 to 3.339 kJ/mol confirming that the adsorption process is physisorption.

5. Comparison of BCG uptake by different adsorbents

Table 5 summarizes a comparative assessment of the adsorption capacities of BCG onto different adsorbents. Compared to other adsorbents, the prepared SWI-FA based geopolymer adsorbent cured at 90^0 C (GP90) in this study had a relatively high adsorption capacity for BCG of 515.5 mg/g. Moreover, the GP90 treated effluent was analyzed for heavy metals leaching (Pb, Cu, Cd, Mn, Cr, Fe and Zn) from the adsorbent into the solution using ICP-OES. The heavy metals were below the instrumental detection limits (10 μg/L), indicates SWI-FA based geopolymer adsorbents immobilized any toxic heavy metals present in SWI-FA and poses no secondary pollution threat, if any.

6. Conclusion

Alkaline activation of otherwise toxic solid waste incinerator fly ash (SWI-FA) was used to produce geopolymer adsorbents at different curing temperatures of 30^0 C (GP30), 50^0 C (GP50), 70^0 C (GP70) and 90^0 C (GP90). The changes in adsorption bands in FT-IR, decrease in degree of crystallinity, disappearance of some mineral phases and formation of new ones are positive evidences for successful geopolymerization. The physico-chemical analysis revealed that increase in curing temperature had a significant effect on structural, morphological and composition of the SWI-FA-based geopolymers that impacted their adsorption capabilities for anionic bromocresol green (BCG) dye. Precisely, the increase in curing temperature resulted in increase in adsorption capacity from 41.70 mg/g to 515.5 mg/g for GP30 and GP90, respectively. The adsorption kinetics of BCG onto the geopolymers followed the pseudo-second-order kinetic law. The adsorption equilibrium data were best described by the isotherms in the order Langmuir> Freundlich>Temkin >D-R-K model. Thermodynamic studies reveal that adsorption is a spontaneous, exothermic and enthalpy-driven process. The adsorption mechanism was a physical process involving electrostatic and hydrogen-bonding interactions. Geopolymer development from SWI-FA for water treatment provides opportunity for the valorization of MWI-FA besides other possible applications.

Table 5
Comparison of BCG uptake by SWI-FA based geopolymers with other adsorbents.

Adsorbent	Adsorption capacity (mg/g)	Time (min)	Reference
Ziziphus mummularia	19.61	8	[9]
ADFS	36.91	100	[31]
Modified PEPP	52.63	90	[37]
$CoFe_2O_4$NHS-250	85.91	10	[38]
AFRH	139.23	40	[40]
TiO_2 brokite nanoparticles	45.5	41	[41]
GP90	515.5	60	This study
GP70	452.5	60	This study
GP50	121.8	60	This study
GP30	41.70	60	This study

Funding

This work was funded by Kaimosi Friends University Grant (KAF/601/APPL/043/1(6)).

CRediT authorship contribution statement

Eugene Owino: Conceptualization, Visualization, Methodology, Writing – original draft. **Victor O. Shikuku:** Conceptualization, Methodology, Writing – review & editing, Supervision, Resources mobilization including funding. **Wilfrida Nyairo:** Writing – review & editing, Supervision, characterization. **Benton Onyango Otieno:** Writing – review & editing, materials characterization. **Chrispin Kowenje:** Conceptualization, Visualization, Methodology, Writing – review & editing, Supervision.

Declaration of Competing Interest

The authors declare that they have no known competing financial interests or personal relationships that could have appeared to influence the work reported in this paper.

Data availability

Data will be made available on request.

Acknowledgement

The authors would like to thank Dr. Pierre Kalenga Mubiayi for his assistance on XRD analysis. Technical supports from Maseno University

(Kenya) and University of Witwatersrand (South Africa) are gratefully acknowledged.

References

[1] S. Tome, H. Dzoujo, V. Shikuku, S. Otieno, Synthesis, characterization and application of acid and alkaline activated volcanic ash-based geopolymers for adsorptive remotion of cationic and anionic dyes from water, Ceram. Int. 47 (15) (2021) 20965–20973, https://doi.org/10.1016/j.ceramint.2021.04.097.

[2] D. Hermann, V.O. Shikuku, S. Tome, S. Akiri, Synthesis of pozzolan and sugarcane bagasse derived geopolymer-biochar composites for methylene blue sequestration from aqueous medium, J. Environ. Manag. 318 (4) (2022), 115533, https://doi.org/10.1016/j.jenvman.2022.115533.

[3] V.O. Shikuku, S. Tome, T.H. Dzoujo, G. Tompsett, M. Timko, Rapid adsorption of cationic methylene blue dye onto volcanic ash-metakaolin based geopolymers, Silicon 14 (15) (2022) 9349–9359, https://doi.org/10.1007/s12633-021-01637-9.

[4] A.A. Siyal, M.R. Shamsuddin, M.I. Khan, N.E. Rabat, M. Zulfiqar, Z. Man, J. Siame, K.A. Azizli, A review on geopolymers as emerging materials for the adsorption of heavy metals and dyes, J. Environ. Manag. 224 (2018) 327–339, https://doi.org/10.1016/j.jenvman.2018.07.046.

[5] Q. Qiu, X. Jiang, G. Lv, Z. Chen, S. Lu, M. Ni, J. Yan, X. Deng, Adsorption of heavy metal ions using zeolite materials of municipal solid waste incineration fly ash modified by microwave-assisted hydrothermal treatment, Powder Technol. 335 (2018) 156–163, https://doi.org/10.1016/j.powtec.2018.05.003.

[6] I. Khan, K. Saeed, I. Zekker, B. Zhang, A.H. Hendi, A. Ahmad, S. Ahmad, N. Zada, H. Ahmad, L.A. Shah, T. Shah, I. Khan, Review on Methylene Blue: its properties, uses, toxicity and photodegradation, Water 14 (2022) 242. https://doi.org/10.3390/w14020242.

[7] L. Liu, Z. Chen, J. Zhang, D. Shan, Y. Wu, L. Bai, B. Wang, Treatment of industrial dye wastewater and pharmaceutical residue wastewater by advanced oxidation processes and its combination with nanocatalysts: a review, J. Water Process Eng. 42 (2021), 102122, https://doi.org/10.1016/j.jwpe.2021.102122.

[8] M.A. Badawi, N.A. Negm, M.T.H. Abou Kana, H.H. Hefni, M.A. Moneem, Adsorption of aluminum and lead from wastewater by chitosan-tannic acid modified biopolymers: isotherms, kinetics, thermodynamics and process mechanism, Int. J. Biol. Macromol. 99 (2017) 465–476, https://doi.org/10.1016/j.ijbiomac.2017.03.003.

[9] A. Shokrollahi, A. Alizadeh, Z. Malekhosseini, M. Ranjbar, Removal of bromocresol green from aqueous solution via adsorption on Ziziphus nummularia as a new, natural, and low-cost adsorbent: kinetic and thermodynamic study of removal process, J. Chem. Eng. Data 56 (10) (2011) 3738–3746, https://doi.org/10.1021/je200311y.

[10] E. Ngeno, E. Mbuci, M. Necibi, V.O. Shikuku, C. Olisah, R. Ongulu, H. Matovu, P. Ssebugere, A. Abushaban, M. Sillanpaa, Sustainable re-utilization of waste materials as adsorbents for water and wastewater treatment in Africa: recent studies, research gaps, and way forward for emerging economies, Environ. Adv. 9 (2022), 100282, https://doi.org/10.1016/j.envadv.2022.100282.

[11] D. Hermann, S. Tome, V.O. Shikuku, J.B. Tchuigwa, A. Spieß, C. Janiak, M.A. Etoh, Enhanced performance of hydrogen peroxide modified pozzolan-based geopolymer for abatement of methylene blue from aqueous medium, Silicon 14 (10) (2021) 5191–5206, https://doi.org/10.1007/s12633-021-01264-4.

[12] M.A. Al-Ghouti, M. Khan, M.S. Nasser, K. Al Saad, O. Ee, Heng, Application of geopolymers synthesized from incinerated municipal solid waste fly ashes for the removal of cationic dye from water, PLoS One 15 (11) (2020), e0239095, https://doi.org/10.1007/journal.pone.0239095.

[13] M. Margallo, M.B.M. Taddel, A. Hernandez-Pellon, R. Aldaco, A. Irabien, Environmental sustainability assessment of the management of municipal solid waste incineration residus: a review of the current situation, Clean. Technol. Environ. Policy 17 (2015) 1333–1353, https://doi.org/10.1007/s10098-015-0961-6.

[14] A.A. Siyal, M.R. Shamsuddin, N.E. Rabat, M. Zulfiqar, Z. Man, A. Low, Fly ash based geopolymer for the adsorption of anionic surfactant from aqueous solution, J. Clean. Prod. 229 (2019) 232–243, https://doi.org/10.1016/j.jclepro.2019.04.384.

[15] Q. Li, S. Chen, Y. Zhang, Y. Hu, Q. Wang, Q. Zhou, Y. Yan, Y. Liu, D. Yan, Effect of curing temperature on high-strength metakaolin-based geopolymer composite (HMGC) with quartz powder and steel fibers, Materials 15 (11) (2022) 3958, https://doi.org/10.3390/ma15113958.

[16] P. Sajan, T. Jiang, C. Lau, G. Tan, K. Ng, Combined effect of curing temperature, curing period and alkaline concentration on the mechanical properties of fly ash-basedgeopolymer, Clean. Mater. 1 (2021), 100002, https://doi.org/10.1016/j.clema.2021.100002.

[17] S. Tome, M.A. Etoh, J. Etame, K. Sanjay, Characterization and leachability behaviour of geopolymer cement synthesised from municipal solid waste incinerator fly ash and volcanic ash blends, Recycling 3 (4) (2018) 50, https://doi.org/10.3390/recycling3040050.

[18] B.A. Ionescu, A.M. Barbu, A.V. Lăzărescu, S. Rada, T. Gabor, C. Florean, The influence of substitution of fly ash with marble dust or blast furnace slag on the properties of the alkali-activated geopolymer paste, Coatings 13 (2) (2023) 403, https://doi.org/10.3390/coatings13020403.

[19] M. Sivasakthi, R. Jeyalakshmi, Effect of change in the silica modulus of sodium silicate solution on the microstructure of fly ash geopolymers, J. Build. Eng. 44 (2021), 102939, https://doi.org/10.1016/j.jobe.2021.102939.

[20] Z. Hajizadeh, F. Radinekiyan, R. Eivazzadeh-Keihan, A. Maleki, Development of novel and green NiFe2O4/geopolymer nanocatalyst based on bentonite for synthesis of imidazole heterocycles by ultrasonic irradiations, Sci. Rep. 10 (1) (2020) 11671, https://doi.org/10.1038/s41598-020-68426-z.

[21] G.B. Singh, K.V. Subramaniam, Influence of processing temperature on the reaction product and strength gain in alkali-activated fly ash, Cem. Concr. Compos. 95 (2019) 10–18, https://doi.org/10.1016/j.cemconcomp.2018.10.010.

[22] A.M. Al Bakria, H. Kamarudin, M. BinHussain, I.K. Nizar, Y. Zarina, A.R. Rafiza, The effect of curing temperature on physical and chemical properties of geopolymers, Phys. Procedia 22 (2011) 286–291, https://doi.org/10.1016/j.phpro.2011.11.045.

[23] J.S.J. Sindhunata, Van Deventer, G.C. Lukey, H. Xu, Effect of curing temperature and silicate concentration on fly-ash-based geopolymerization, Ind. Eng. Chem. Res. 45 (10) (2006) 3559–3568, https://doi.org/10.1021/ie051251p.

[24] D. Liu, J. Yuan, J. Li, G. Zhang, Preparation of chitosan poly (methacrylate) composites for adsorption of bromocresol green, ACS Omega 4 (7) (2019) 12680–12686, https://doi.org/10.1021/acsomega.9b01576.

[25] V.O. Shikuku, R. Zanella, C.O. Kowenje, Filipe F. Donato, Nelson Bandeira, O. D. Prestes, Single and binary adsorption of sulphonamide antibiotics onto iron-modified clay: linear and nonlinear Isotherms, Kinetics, thermodynamics and mechanistic studies, Appl. Water Sci. 8 (2018) 175, https://doi.org/10.1007/s13201-018-0825-4.

[26] S.K. Lagergren, About the theory of so-called adsorption of soluble substances, Sven. Vetensk. Handingarl 24 (1898) 1–39.

[27] Y. Ho, G. McKay, Pseudo-second order model for sorption processes, Process Biochem. 34 (5) (1999) 451–465, https://doi.org/10.1016/S0032-9592(98)00112-5.

[28] W.J. Weber, J.C. Morris, Kinetics of adsorption on carbon from solution, J. Sanit. Eng. Div. Am. Soc. Civ. Eng. 89 (1963) 31–60, https://doi.org/10.1061/JSEDAI.0000430.

[29] S. Liu, Y. Ding, P. Li, K. Diao, X. Tan, F. Lei, Y. Zhan, Q. Li, B. Huang, Z. Huang, Adsorption of the anionic dye Congo red from aqueous solution onto natural zeolites modified with N, N-dimethyl dehydroabietylamine oxide, Chem. Eng. J. 248 (2014) 135–144, https://doi.org/10.1016/j.cej.2014.03.026.

[30] C. Xiong, S. Wang, L. Zhang, Y. Li, Y. Zhou, J. Peng, Preparation of 2-aminothiazole-functionalized poly (glycidyl methacrylate) microspheres and their excellent gold ion adsorption properties, Polymers 10 (2) (2018) 159, https://doi.org/10.3390/polym10020159.

[31] H. Saad, F.N. El-Dien, N.E. El-Gamel, A.S.A. Dena, Azo-functionalized superparamagnetic Fe 3 O 4 nanoparticles: an efficient adsorbent for the removal of bromocresol green from contaminated water, RSC Adv. 12 (39) (2022) 25487–25499, https://doi.org/10.1039/D2RA03476J.

[32] I. Langmuir, The constitution and fundamental properties of solids and liquids, J. Am. Chem. Soc. 38 (11) (1916) 2221–2295, https://doi.org/10.2121/ja02268a002.

[33] H. Freundlich, Über die adsorption in losungen, Z. Phys. Chem. 57 (4) (1906) 385–470, https://doi.org/10.1515/zpch-1907-5723.

[34] M.M. Dubinin, Generalization of the theory of volume filling of micropores to nonhomogeneous microporous structures, Carbon 23 (4) (1985) 373–380, https://doi.org/10.1016/0008-6223(85090029-6.

[35] M.I. Temkin, Adsorption equilibrium and the kinetics of processes on nonhomogeneous surfaces and in the interaction between adsorbed molecules, Zh. Fiz. Chim. 15 (1941) 296–332.

[36] V.O. Shikuku, T. Mishra, Adsorption isotherm modelling for methylene blue removal onto magnetic kaolinite clay: a comparison of two-parameter isotherms, Appl. Water Sci. 11 (2021) 103, https://doi.org/10.1007/s13201-021-01440-2.

[37] G. Torğut, K. Demirelli, Comparative adsorption of different dyes from aqueous solutions onto polymer prepared by ROP: kinetic, equilibrium and thermodynamic studies, Arab. J. Sci. Eng. 43 (2018) 3503–3514, https://doi.org/10.1007/s13369-017-2947-7.

[38] R. Rakshit, E. Khatun, M. Pal, S. Talukdar, D. Mandal, P. Saha, K. Mandal, Influence of functional group of dye on the adsorption behaviour of CoFe 2 O 4 nano-hollow spheres, New J. Chem. 41 (17) (2017) 9095–9102, https://doi.org/10.1039/C7NJ00941K.

[39] I. Luttah, D. Onunga, V.O. Shikuku, B. Otieno, C. Kowenje, Removal of endosulfan from water by municipal waste incinerator fly ash based geopolymers: adsorption kinetics, isotherms, and thermodynamics, Front. Environ. Chem. 4 (2023) 1164372, https://doi.org/10.3389/fenvc.2023.1164372.

[40] C.E. Onu, B.N. Ekwueme, P.E. Ohale, C.P. Onu, C.O. Asadu, C.C. Obi, O.O. Onu, Decolourization of bromocresol green dye solution by acid functionalized rice husk: artificial intelligence modeling, GA optimization, and adsorption studies, J. Hazard Mater. Adv. 9 (2023), 100224, https://doi.org/10.1016/j.hazadv.2022.100224.

[41] M. Hmoudah, A. El-Qanni, S. Abuhatab, N.N. Marei, A. El-Hamouz, B.J. A. Tarboush, M. Di Serio, Competitive adsorption of Alizarin Red S and Bromocresol Green from aqueous solutions using brookite TiO2 nanoparticles: experimental and molecular dynamics simulation, Environ. Sci. Pollut. Res. 29 (51) (2022) 77992–78008, https://doi.org/10.1007/s11356-022-21368-7.